1   Revision 1

2

3   **Paratobermorite, Ca$_4$(Al$_{0.5}$Si$_{0.5}$)$_2$Si$_4$O$_{16}$(OH)·2H$_2$O·(Ca·3H$_2$O), a new tobermorite-supergroup**

4   **mineral with a novel topological type of the microporous crystal structure**

5

6   Igor V. Pekov[1], Natalia V. Zubkova[1]*, Nikita V. Chukanov[2], Stefano Merlino[3], Vasiliy O.

7   Yapaskurt[1], Dmitry I. Belakovskiy[4], Alexander B. Loskutov[5], Elena A. Novgorodova[6], Svetlana

8   A. Vozchikova[2], Sergey N. Britvin[7] and Dmitry Yu. Pushcharovsky[1]

9

10   [1]Faculty of Geology, Moscow State University, Vorobievy Gory, 119991 Moscow, Russia

11   [2]Institute of Problems of Chemical Physics, Russian Academy of Sciences, 142432 Chernogolovka,

12   Moscow region, Russia

13   [3] Accademia Nazionale dei Lincei, Via della Lungara 10, Roma, Italy

14   [4]Fersman Mineralogical Museum of the Russian Academy of Sciences, Leninsky Prospekt 18-2,

15   119071 Moscow, Russia

16   [5]Voykova str., 62-500, 624266, Asbest, Sverdlovsk Oblast, Russia

17   [6]Voykova str., 67-6, 624266, Asbest, Sverdlovsk Oblast, Russia

18   [7]St. Petersburg State University, University Emb. 7/9, 199034 St. Petersburg, Russia

19

20   *Corresponding author: n.v.zubkova@gmail.com

21

22

23   **ABSTRACT**

24   A   new   mineral   paratobermorite   with   the   ideal   crystal-chemical   formula

25      $Ca_4(Al_{0.5}Si_{0.5})_2Si_4O_{16}(OH)\cdot2H_2O\cdot(Ca\cdot3H_2O)$ is a member of the tobermorite group within the

26   tobermorite supergroup. It was found at the Bazhenovskoe chrysotile asbestos deposit, Central

27   Urals, Russia, in cavities of grossular rodingite in association with prehnite, pectolite, thomsonite-

28   Ca, and calcite. Paratobermorite occurs as well-shaped prismatic to acicular crystals up to $1 \times 1.5 \times$

29   8 mm^3 typically assembled in spray- or bush-like radial clusters or open-work aggregates up to 1.5

30   cm across which form interrupted crusts up to 3×5 cm^2. Paratobermorite is transparent, colorless,

31   pale yellowish, pale beige or pinkish, with vitreous lustre. The mineral is brittle, with the (001)

32   perfect cleavage. The Mohs hardness is *ca*. 3½. $D_{meas.}$ = 2.51 (2) and $D_{calc.}$ = 2.533 g cm^{-3}.

33   Paratobermorite is optically biaxial (+), α = 1.565 (2), β = 1.566 (2), γ = 1.578 (2), $2V_{meas.}$ = 25 (10)^o

34   and $2V_{calc.}$ = 32° (589 nm). Optical orientation is: $X = c$, $Y = b$, $Z = a$. The chemical composition of

35   paratobermorite (electron microprobe, H_2O by selective sorption from gaseous products of heating)

36   is: Na_2O 0.40, K_2O 0.28, CaO 36.60, MnO 0.04, BaO 0.07, Al_2O_3 6.46, SiO_2 42.32, H_2O 14.10, total

37   100.27 wt.%. The empirical formula calculated on the basis of 22 O atoms per formula unit and

38      $(O,OH)_{17}\cdot5H_2O$ is $Na_{0.09}K_{0.04}Ca_{4.72}Al_{0.92}Si_{5.09}O_{15.69}(OH)_{1.31}\cdot5H_2O$. As all the other members of the

39   tobermorite supergroup, paratobermorite displays OD character, with two MDO (maximum degree

40   of order) structures, one (MDO1), with non-standard space group $F2/d11$ and the second (MDO2),

41   just corresponding to the structure-type of the new mineral, with non-standard space group

42      $C112_1/m;$ its unit-cell parameters obtained from single-crystal X-ray diffraction data are: a =

43   11.2220 (4), b = 7.3777 (2), c = 22.9425 (8) Å, γ = 89.990 (3)^o, V = 1899.46 (10) Å^3, and Z = 4;

44   polytype $2M$. The crystal structure of paratobermorite is solved on single crystal, R = 8.36%. Like

45   structures of other 'tobermorites 11 Å', it is based on the complex layer built of sheet of seven-fold

46   Ca-centred polyhedra with wollastonite-type chains of T tetrahedra attached to Ca-sheet from both

47 sides. The tetrahedral (T) sites T1 and T2 are fully occupied by Si while alternating T3 and T4 sites

48 are filled by Al and Si in the ratio 1:1. The chains of tetrahedra belonging to neighboring complex

49 layers share common oxygen vertices of the bridging T3,4 tetrahedra to form xonotlite-type ribbons

50 $[Si_6O_{17}]^\infty$. The heteropolyhedral Ca-T-O scaffolding appears as a microporous quasi-framework with

51 wide channels which contain additional Ca atoms and H_2O molecules. The complex Ca-T-O layers

52 in paratobermorite (so-called *complex modules of type A*) significantly differ in topology (mutual

53 arrangement of T tetrahedra and Ca polyhedra) from the complex Ca-T-O layers in tobermorite

54 (*complex modules of type B*). The IR spectrum confirms the presence of nonequivalent H_2O

55 molecules and nonequivalent T–O–T angles involving T atoms of two neighboring wollastonite-type

56 chains. Due to the original topological type of the structure and the presence of significant amount

57 of Al which substitutes Si, paratobermorite can be considered as a novel microporous material, a

58 perspective cation-exchanger.

59

60 **Keywords**: paratobermorite, tobermorite group, new mineral, calcium silicate hydrate, OD

61 character, crystal structure, IR spectroscopy, Portland cement, ion exchanger, rodingite,

62 Bazhenovskoe deposit

63

3

64

INTRODUCTION

66

67   Tobermorite-supergroup members (or 'tobermorites') belong to a large family of calcium

68   silicate hydrate (C-S-H) compounds, which includes many natural and synthetic representatives. For

69   many years, 'tobermorites' have been in the focus of research by crystal chemists and material

70   scientists due to their close relationships with the C-S-H compounds formed during the Portland

71   cement hydration (Richardson 2008). In addition, 'tobermorites' demonstrate cation exchange

72   properties and can be used in waste disposal (Bonaccorsi and Merlino 2005). Natural 'tobermorites'

73   are united in the tobermorite supergroup. Until recently, this supergroup included five mineral

74   species: tobermorite, kenotobermorite (forming the tobermorite group), clinotobermorite,

75   plombiérite, and riversideite (Biagioni et al. 2015; see below for details).

76   In this paper we describe a new representative of the tobermorite group which differs from

77   other members of the tobermorite supergroup not only in chemical features, symmetry and unit-cell

78   metrics but also in the topology of the crystal structure, which is the most significant individual

79   feature of the new mineral. It is named **paratobermorite** from the Greek παρα for "near" and the

80   relationship to tobermorite. Both the new mineral and its name have been approved by the

81   Commission on New Minerals, Nomenclature and Classification of the International Mineralogical

82   Association (IMA No. 2020–100). The type specimen is deposited in the systematic collection of the

83   Fersman Mineralogical Museum of the Russian Academy of Sciences, Moscow under the catalogue

84   number 97513.

85

86   **TOBERMORITE-SUPERGROUP MINERALS:**

87   **HISTORICAL BACKGROUND AND GENERAL CRYSTAL CHEMICAL FEATURES**

88

4

89   Historically, among 'tobermorites' three types of minerals, so-called tobermorites 14 Å, 11 Å,

90   and 9 Å were distinguished in correspondence with the strongest basal d-spacing in a powder X-ray

91   diffractogram. In terms of mineral names, they correspond to plombiérite, tobermorite, and

92   riversideite, respectively (Taylor 1953, 1964; McConnell 1954). The name tobermorite was

93   introduced in the mineralogy by Heddle (1880), for a new mineral described from four localities in

94   Scotland, including three near Tobermory. Claringbull and Hey (1952), who re-examined the

95   Heddle's material, found that tobermorite is an individual natural C-S-H phase, which demonstrates

96   the main basal reflection of powder X-ray diffraction (XRD) pattern with $d = 11.3$ Å. Based on this,

97   McConnell (1954) applied the mineral name tobermorite to the C-S-H compounds with a 11 Å main

98   basal spacing.

99   The structure model for tobermorite (tobermorite $s.s.$, or 'tobermorite 11 Å') was firstly

100   suggested by Megaw and Kelsey (1956) and later elaborated by Mamedov and Belov (1958) and

101   Hamid (1981). The real structure of 'tobermorite 11 Å', its structural variations and polytypism were

102   studied by Merlino et al. (1999, 2001) and Merlino and Bonaccorsi (2008). Hydrogen-bearing

103   groups in one of varieties of 'tobermorite 11 Å' were examined in detail by Churakov (2009).

104   Clinotobermorite, a natural C-S-H phase with a 11 Å main basal d-spacing, dimorphous with

105   tobermorite, was described as a new mineral species from Fuka, Okayama Prefecture, Japan (Henmi

106   and Kusachi, 1992). Its sub-cell structure was determined by Hoffmann and Armbruster (1997),

107   whereas the real structure was defined by Merlino et al. (2000).

108   In 2015, the IMA-approved nomenclature of the tobermorite supergroup was published. In

109   the frame of this nomenclature (Biagioni et al. 2015), five valid mineral species were distinguished

110   and clearly defined. 'Tobermorites 14 Å' are represented by plombiérite with the idealized, end-

111   member formula $Ca_5Si_6O_{16}(OH)_2 \cdot 7H_2O$, 'tobermorites 9 Å' by riversideite with the end-member

112   formula $Ca_5Si_6O_{16}(OH)_2$ and 'tobermorites 11 Å' include three species. Tobermorite and

113   clinotobermorite are defined as dimorphs with the idealized, end-member formula $Ca_5Si_6O_{17}\cdot5H_2O$.

114   Besides this pair, 'tobermorites 11 Å' include kenotobermorite with the end-member formula

115    $Ca_4Si_6O_{15}(OH)_2\cdot5H_2O$ (Table 1).

116   The fundamental building unit in the crystal structure of all tobermorite-supergroup minerals

117   is the complex module (or complex layer) consisting of a sheet of seven-coordinated Ca-centred

118   polyhedra decorated from both sides by Si-centred tetrahedra (*T*) belonging to wollastonite-type

119   chains $[Si_3O_9]^\infty$ (Merlino and Bonaccorsi 2008). This complex module is *C*-centred and has the

120   periods $a \approx 11.2$ Å, $b \approx 7.3$ Å and thickness $c_0 \approx 11.2$ Å (Merlino et al. 1999, 2000, 2001; Biagioni

121   et al. 2015). In Fig. 1, the complex module is illustrated by the examples taken from 'tobermorites 11

122   Å'. As distinct from plombiérite, in 'tobermorites 11 Å' the stacking of the complex modules gives

123   rise to the condensation of wollastonite-type chains of tetrahedra to form the $[Si_6O_{17}]^\infty$ double chains

124   (Merlino and Bonaccorsi 2008), also known as xonotlite-type ribbons. In cavities (channels) within

125   the resulting heteropolyhedral Ca-*T*-O quasi-framework, additional cations (typically, Ca, up to one

126   atom per formula unit, below *apfu*) and H_2O molecules occur (Fig. 2). In particular, the presence or

127   absence of Ca in these cavities is a cause of the difference in the number of Ca *apfu* between

128   tobermorite $Ca_5Si_6O_{17}\cdot5H_2O$ and kenotobermorite $Ca_4Si_6O_{15}(OH)_2\cdot5H_2O$ (Biagioni et al. 2015). The

129   presence of these wide channels confers the properties of 'tobermorites' as ion-exchangers.

130   Bonaccorsi and Merlino (2005) stressed that there are two geometrically distinct ways to

131   place the chains of tetrahedra on the two sides of the calcium sheet in the complex module. In the

132   first one, the bridging tetrahedra are placed at right on one side and at left on the other side (or vice

133   versa), with respect to the disilicate groups of the corresponding chain. Such layer was marked as

134   *complex module of type A*. In the second way, the bridging tetrahedra on both sides are all placed at

135   left (or all placed at right) with respect to the corresponding disilicate groups. The layer of this type

136   was called *complex module of type B* (Bonaccorsi and Merlino 2005; Biagioni et al. 2015). Thus, the

6

137   complex modules of types A and B are topologically different (Fig. 1). The complex module of type

138   B is known in tobermorite and kenotobermorite, whereas the complex module of type A is known in

139   clinotobermorite. Now it is found in paratobermorite.

140

141   **POLYTYPIC ASPECTS IN TOBERMORITE GROUP OF MINERALS**

142

143   The various members of the 'tobermorite supergroup' present an order-disorder (OD)

144   character (Dornberger-Schiff 1956, 1964, 1966; Ferraris et al. 2008) related to the metrical

145   relationships between the calcium polyhedral module, with a repeat of 3.56 Å, and the wollastonite-

146   type chains, with a periodicity of 7.3 Å. The chains may be connected to the calcium layers in two

147   distinct but equivalent positions, shifted by 3.65 Å in the **b** direction. Consequently, the various

148   phases of the tobermorite supergroup can be described in terms of OD layers which may stack in

149   two different ways along **c***, giving rise to a whole family of disordered or ordered sequences

150   (polytypes).

151   In all the polytypes of a family (but also in the disordered sequences) pairs of adjacent

152   layers are geometrically equivalent (principle of OD structures). In each family two main polytypes

153   exist, corresponding to the sequences in which not only pairs but also triples, quadruples,… n-tuples

154   of layers are geometrically equivalent, corresponding to the MDO (Maximum Degree of Order)

155   structures.

156   In the case of tobermorite (tobermorite 11Å), kenotobermorite and paratobermorite the OD

157   layer (Fig. 3) presents layer symmetry $C2m(m)$ (one of the possible eighty layer groups), with

158   translation vectors **a** and **b**, third vector $\mathbf{c_0}$ ($a \sim 11.3$, $b \sim 7.35$, $c_0 \sim 11.2$ Å). The parentheses in the

159   last position of the symbol for the layer group indicate the direction of missing periodicity.

160   For a layer with symmetry $C2m(m)$ there are two possible sets of σ-operations (operations

161   which relate adjacent layers) compatible with the set of λ-operations (Ferraris et al. 2008)

7

162   C 2 m (m) C 2 m (m) (1)

163   { 2_s $n_{2,s}$ $(n_{s,r})$ }   { $n_{r,2}$ 2_r (2_2) }

164

165   The first of them, with value ½ for both s and r parameters, results in the OD groupoid

166   family symbol

167   C 2 m (m)

168   { $2_{1/2}$ $n_{2,1/2}$ $(n_{1/2,1/2})$ }

169   which just consents the derivation of the real structure of tobermorite and kenotobermorite and the

170   definition of their two main polytypes (MDO structures) (Merlino et al. 1999; 2001; Biagioni et al.

171   2015).

172   It seems proper to recall that the symbols used for the σ-operations are in keeping with those

173   used in the normal space group operations: $2_{1/2}$ represents a rotation of 180° followed by translation

174   along **a** of $a/4$; $n_{2,1/2}$ represents a glide normal to **b** with translational components c_0 and $a/4$; $n_{1/2,1/2}$

175   represents a glide normal to c_0, with translational components **a**/4 and **b**/4.

176   Layers of $C2mm$ symmetry follow each other in the **c** direction, related by the operator $n_{1/2,1/2}$ (= $n_{-1/2,-1/2}$ due to the C centring of the single layer) normal to **c**, or by the operator $n_{1/2,-1/2}$ (= $n_{-1/2,1/2}$).

178   The polytype MDO1 corresponds to the sequence in which the operators $n_{1/2,1/2}$ and $n_{1/2,-1/2}$

179   regularly alternate, resulting in a structure with $F2dd$ symmetry and cell parameters $a \sim 11.3$, $b \sim$

180   7.35, $c \sim 45.2$ Å (Merlino et al., 2001). MDO2 corresponds to the sequence in which the operator

181    $n_{1/2,1/2}$ is constantly applied, resulting in a structure with C centred cell, with parameters $a \sim 11.3$, b

182   ~ 7.35, $c \sim 22.6$ Å, $\gamma \sim 90°$, presenting additional lattice points at ¼, ¼, ½ and ¾, ¾, ½ (Fig. 3 in

183   Merlino et al., 2001). A convenient cell may be derived through the transformations **a'** = (**a** + **b**)/2,

184   **b'** = **b**, **c'** = c , thus obtaining a B centred monoclinic cell, space group $B11m$ and cell parameters

185    $a \sim 6.73$, $b \sim 7.35$, $c \sim 22.6$ Å, $\gamma \sim 122.9°$.

8

186   In a paper by Merlino and Bonaccorsi (2008), attention has been given to the second set of

187   σ-operations compatible with the layer group symmetry $C2m(m)$. By assuming the value ½ for the r

188   parameter a new OD groupoid family was obtained which has the symbol

189   C 2 m (m)

190                          $\{\, n_{1/2,2} \quad 2_{1/2} \quad (2_2)\, \}$

191   and by which a new family of OD structures may be obtained.

192   Merlino and Bonaccorsi (2008) indicated that also in the present case two main polytypes

193   exist: MDO1 is obtained through the constant application of the $[n_{1/2,2}$ - -$]$ operation and presents

194   non-standard space group $F2/d11$, with $a = 11.3$, $b = 7.35$, $c = 45.2$ Å, $\alpha = 90°$; MDO2 is obtained

195   through the regular alternation of the operations $[n_{1/2,2}$ - -$]$ and $[n_{-1/2,2}$ - -$]$ and presents non-standard

196   space group $C112_1/m$, with $a = 11.3$, $b = 7.35$, $c = 22.6$ Å, $\gamma = 90°$. The unit cell dimensions, space

197   group and structural arrangement of the last polytype closely correspond to those of

198   paratobermorite, the mineral species described in the present paper.

199   Tobermorite and kenotobermorite share the same OD family, but show distinguished

200   chemical composition, $Ca_5Si_6O_{17}\cdot 5H_2O$ for tobermorite and $Ca_4Si_6O_{15}(OH)_2\cdot 5H_2O$ for

201   kenotobermorite. As regards the polytypic aspects both main polytypes of kenotobermorite have

202   been observed in nature: kenotobermorite-2M ($B11m$, $a = 6.735$, $b = 7.385$, $c = 22.487$ Å, $\gamma =$

203   123.25°) and kenotobermorite-4O ($F2dd$, $a = 11.265$, $b = 7.385$, $c = 44.97$ Å), respectively; whereas

204   only the monoclinic polytype tobermorite-2M ($B11m$, $a = 6.732$, $b = 7.369$, $c = 22.680$ Å, $\gamma =$

205   123.18°) has been found. Paratobermorite, $Ca_5AlSi_5O_{16}(OH)\cdot 5H_2O$ has a peculiar OD character,

206   pertaining to a different OD family. Similar to the case of tobermorite, so far only the polytype

207   paratobermorite-2M has been found in nature.

208

209   **ANALYTICAL METHODS AND DATA PROCESSING DETAILS**

210

211   The chemical composition of paratobermorite was determined by electron microprobe in the

212   Laboratory of Analytical Techniques of High Spatial Resolution, Dept. of Petrology, Moscow State

213   University (MSU) using a Jeol JSM-6480LV scanning electron microscope (SEM) equipped with an

214   INCA-Wave 500 wavelength-dispersive spectrometer, with an acceleration voltage of 20 kV, a

215   beam current of 10 nA; the electron beam was rastered to the 5×5 μm^2 area. The standards used are

216   listed in Table 2. The studies of morphology of paratobermorite crystals and aggregates, including

217   the obtaining of SEM images, were carried out using the same scanning electron microscope.

218   H_2O was determined by the Alimarin method [the Penfield method modified for small

219   samples and involving selective sorption of H_2O on $Mg(ClO_4)_2$ from gaseous products obtained by

220   heating the mineral at 1080°C in oxygen at 1 atm]. Two measurements were performed and the

221   results were averaged. The attempt to measure CO_2 content was made using the method of selective

222   sorption of CO_2 on askarite (an asbestiform material saturated with NaOH) from gaseous products

223   obtained by heating the mineral at 1080°C in oxygen at 1 atm. This experiment showed the absence

224   of CO_2 in paratobermorite (that is in agreement with both IR spectroscopy and structure data: see

225   below).

226   In order to obtain infrared (IR) absorption spectrum, powdered sample of paratobermorite was

227   mixed with anhydrous KBr, pelletized, and analyzed using an ALPHA FTIR spectrometer (Bruker

228   Optics) at a resolution of 4 cm^{-1}. A total of 16 scans were collected. The IR spectrum of an analogous

229   pellet of pure KBr was used as a reference. A sample of tobermorite (tobermorite-2*M*) from the

230   Pervomaiskiy quarry, Mt. Bol'shoy Kermen, Bakhchisaray district, Crimea Peninsula was prepared

231   and studied using the same procedures for comparison.

232   Powder XRD study of paratobermorite was carried out using a Rigaku R-AXIS Rapid II

233   single-crystal diffractometer equipped with a curved image plate detector (Debye-Scherrer

234   geometry, *r* = 127.4 mm) and Co*K*α radiation source (rotating anode; 40 kV, 15 mA, and 12 min

235   exposure time; powdered sample of spherical form prepared with X-ray amorphous glue was studied

236   ), with Rigaku VariMax microfocus mirror optics. Imaging plate-to-profile data conversion was

237   performed using osc2xrd software (Britvin et al. 2017).

238   Single-crystal XRD studies of paratobermorite were carried out on a crystal of $0.21 \times 0.30 \times$

239   0.63 mm^3 in size using an Xcalibur S single-crystal diffractometer equipped with a CCD detector. A

240   full sphere of three-dimensional data was collected. Data reduction was performed using

241   CrysAlisPro version 1.171.39.46 (Rigaku OD 2018). The data were corrected for Lorentz factor and

242   polarization effect.

243   The crystal structure of paratobermorite was solved by direct methods and refined using the

244   SHELX software package (Sheldrick 2015) to $R = 0.0831$ for 2076 unique reflections with $I > 2\sigma(I)$

245   in the frame of monoclinic space group $P2_1/m$ [unit-cell parameters: $a = 6.7149(2)$, $b = 22.9441(8)$,

246    $c = 6.7162(3)$ Å, $\beta = 113.358(4)°$]. In this setting, the a and c parameters of the unit cell have nearly

247   the same values, and the transition to a pseudo-orthorhombic unit cell can be performed by applying

248   the matrix 1 0 -1 / 1 0 1 / 0 -1 0. The unit cell obtained in that way is comparable with those

249   suggested for tobermorite ('tobermorite 11 Å') and other closely related tobermorite-supergroup

250   minerals reported in recent papers (Merlino et al. 1999, 2000, 2001; Merlino and Bonaccorsi 2008;

251   Biagioni et al. 2015): see Table 1. We have re-integrated single-crystal XRD data and refined the

252   structure model of paratobermorite in the non-standard space group $C112_1/m$ to $R = 0.0836$ for 2055

253   unique reflections with $I > 2\sigma(I)$. For an easier comparison, $C112_1/m$ is chosen by us as the "natural"

254   space group for paratobermorite, consenting an easy comparison with the other 'tobermorite 11 Å'

255   phases (Table 1). In both structure models of paratobermorite, microtwinning was observed. The

256   transition matrices 0 0 1 / 0 -1 0 / 1 0 0 (sp. gr. $P2_1/m$) and -1 0 0 / 0 1 0 / 0 0 1 (sp. gr. $C112_1/m$) are

257   found, and the refined twin ratio is 0.53 : 0.47. Complete sets of crystallographic data for both

11

258   models, with the space groups $P2_1/m$ and $C112_1/m$, can be retrieved from the CIF files attached as

259   the Supplementary Material.

260   All attempts to obtain a reasonable structure model for paratobermorite in the frame of

261   orthorhombic symmetry unit cell were unsuccessful. The *PLATON* program (Spek 2003) did not

262   detect higher metrics or crystallographic symmetry for the monoclinic model.

263

264   **RESULTS AND DISCUSSION**

265   **Occurrence**

266   Paratobermorite was found at the Bazhenovskoe deposit of chrysotile asbestos located at the

267   eastern border of the city of Asbest, Sverdlovsk Oblast, Central (Middle) Urals, Russia.

268   The Bazhenovskoe deposit related to the Bazhenovsky gabbro-harzburgite intrusion is one of

269   the world-largest deposits of high-quality chrysotile asbestos. It was discovered in 1885 and is

270   operated since 1889. From the mineralogical viewpoint, Bazhenovskoe is mainly known due to

271   rodingites formed as a result of a low-grade metamorphism after numerous gabbro dikes hosted by

272   serpentinites. Geological and mineralogical data on Bazhenovskoe rodingites were summarized by

273   Erokhin (2017).

274   One of the bright mineralogical features of the Bazhenovskoe deposit is the abundance and

275   diversity of C-S-H minerals in late, hydrothermal parageneses related to rodingites. Some of them

276   are known here in the form of large and perfect crystals, which is unusual for these minerals. The

277   studies of samples from Bazhenovskoe gave a significant contribution to the mineralogy and crystal

278   chemistry of calcium silicate hydrates, namely tobermorite, plombiérite (Zadov et al. 1995, 2001;

279   Merlino et al. 2001), rosenhahnite (Zadov et al. 2000), and oyelite (Pekov et al. 2019). The

280   discovery of paratobermorite again highlights the important role of the Bazhenovskoe deposit for the

281   mineralogy of calcium silicate hydrates.

282   The specimens with the new mineral were collected in 2019 from a rodingite vein uncovered

283   in the eastern part of the Southern open pit operating on the Bazhenovskoe deposit. This steeply

284   dipping (with the dipping angle of 70–80º) vein about 0.5 m thick is seated in serpentinites and has a

285   near-meridional orientation. In the area where paratobermorite was found, the main rodingite-

286   forming mineral is white, colorless or grayish massive, fine-grained grossular and the subordinate

287   mineral is prehnite. Paratobermorite occurs in cavities together with pectolite (represented by both

288   1A and $M2abc$ polytypes), thomsonite-Ca, and calcite. Paratobermorite is a hydrothermal mineral

289   crystallized in a Ca-rich assemblage related to rodingite, a rock formed as a result of metasomatic

290   alteration (rodingitization) of a gabbroid dyke cross-cutting serpentinite (Erokhin 2017 and

291   references therein).

292

293   General appearance, crystal morphology, physical properties and optical data

294   Paratobermorite forms prismatic to acicular crystals, elongated along [010], up to 1 mm ×

295   1.5 mm × 8 mm. They are well-shaped, perfectly terminated (Figs. 4 and 5a,b) or crude (Fig. 5c),

296   sometimes divergent, and typically assembled in open-work aggregates (Figs. 5c and 6a) up to 1 cm

297   × 1.5 cm, spray- or bush-like radial clusters (Fig. 6b) up to 1.3 cm across. Crystal crusts, usually

298   interrupted, of paratobermorite up to 3 cm × 5 cm in area and up to 1 cm thick cover grossular and

299   prehnite aggregates whereas pectolite, thomsonite-Ca and calcite overgrow paratobermorite.

300   Noteworthy, unlike other 'tobermorites', which typically occur (in particular, at

301   Bazhenovskoe) as thin acicular to hair-like individuals (tobermorite, clinotobermorite) or scales

302   (plombiérite), paratobermorite forms relatively thick prismatic crystals (Figs. 4–6). The prismatic

303   zone of paratobermorite crystals is formed by the {100} and {001} faces and the terminations are

304   formed by the {011} faces (Fig. 4: the pseudo-orthorhombic setting with γ = 90º is used). Contact

305   twins on {100} were observed under the microscope in polarized transmitted light; microtwinning

306 with the same plane (100) as a twinning operator (the matrix is -1 0 0 / 0 1 0 / 0 0 1) was found

307 during the crystal structure determination.

308 Paratobermorite is transparent, colorless, pale yellowish, pale beige or pinkish, with white

309 streak and vitreous lustre. The mineral does not fluoresce in ultraviolet light. Paratobermorite is

310 brittle, the (001) perfect cleavage is observed, and the fracture is stepped. The Mohs hardness is *ca*.

311 3½. Density measured by flotation in heavy liquids (bromoform + heptane) is equal to 2.51 (2) g

312 cm^{-3}. Density calculated using the empirical formula and unit-cell volume determined from the

313 single-crystal XRD data is 2.533 g cm^{-3}.

314 Under the microscope, in plane polarized transmitted light paratobermorite is colorless and

315 non-pleochroic. It is optically biaxial (+), α = 1.565 (2), β = 1.566 (2), γ = 1.578 (2), $2V_{meas.}$ = 25

316 (10)º and $2V_{calc.}$ = 32º (589 nm). Dispersion of optical axes was not observed. Extinction is parallel

317 and elongation is negative. Orientation is as follows: $X = c$, $Y = b$, $Z = a$.

318

Chemical composition

320 The chemical composition of paratobermorite in wt.% is given in Table 2. The charge-

321 balanced empirical formula calculated on the basis of 22 O atoms per formula unit (*apfu*) and

322 $(O,OH)_{17} \cdot 5H_2O$ *pfu* (in accordance with structural data, see below) is

323 $Na_{0.09}K_{0.04}Ca_{4.72}Al_{0.92}Si_{5.09}O_{15.69}(OH)_{1.31} \cdot 5H_2O$. The simplified formula is $Ca_5AlSi_5O_{16}(OH) \cdot 5H_2O$.

324 The ideal crystal-chemical formula of paratobermorite written in accordance with the scheme

325 proposed in the frame of the IMA-accepted nomenclature of tobermorite-supergroup minerals

326 (Biagioni et al. 2015) is $Ca_4(Al_{0.5}Si_{0.5})_2Si_4O_{16}(OH) \cdot 2H_2O \cdot (Ca \cdot 3H_2O)$ (see structure data below).

327 The compatibility index $1 - (K_p/K_c) = -0.008$ if $D_{meas.}$ is used and $= 0.001$ if $D_{calc.}$ is used.

328 Both values are rated as *superior*, according to Mandarino (1981).

329

14

330   **Infrared spectroscopy**

331

332   In the IR spectra of paratobermorite and tobermorite (Fig. 7), absorption bands are observed in

333   the ranges of 3200–3600 cm^{-1} (O–H stretching vibrations, 1620–1650 cm^{-1} (H–O–H bending

334   vibrations of H_2O molecules), 920–1220 cm^{-1} (Si–O stretching vibrations), 870–910 cm^{-1} (stretching

335   vibrations involving Al–O bonds), 650–770 cm^{-1} (Ca$\cdots$O–H and/or O–T–O bending vibrations) and

336   below 600 cm^{-1} (lattice modes involving Si–O stretching, Si–O–Si bending and H_2O librational

337   vibrations). For the assignment of the IR bands see (Zadov et al. 2001, 2006; Organova et al. 2002;

338   Chukanov and Chervonnyi 2016).

339   The main differences between the IR spectra of tobermorite and paratobermorite are observed in the

340   ranges of 650–770, 870–910, 1100–1220, and 3200–3600 cm^{-1} which may be due to significant

341   differences between these minerals in the Al:Si ratio, stacking of wollastonite-type chains, and

342   hydrogen bonding. In particular, the strong IR band at 878 cm^{-1} is a specific feature of paratobermorite.

343   This band is not observed in IR spectra of Al-poor tobermorite-group minerals.   As it was shown

344   earlier (Chukanov 2014), in silicates with polymerized SiO_4 tetrahedra, the position of the most

345   high-frequency Si–O-stretching band, $\nu_{Si-O}(max)$, observed in the range of 1000–1220 cm^{-1},

346   depends on the value of the greatest Si–O–Si angle, φ_{SiOSi}. At $\varphi_{SiOSi} = 180°$ the value $\nu_{Si-O}(max)$ is

347   close to 1200 cm^{-1}. For example, in the IR spectrum of xonotlite (with $\varphi_{SiOSi} = 180°$ at the stacking

348   of wollastonite-type chains: see Kudoh and Takeuchi 1979) $\nu_{Si-O}(max)$ is equal to 1203 cm^{-1}. The

349   crystal structure of tobermorite is also based on xonotlite-like ribbons with the φ_{SiOSi} angle close to

350   180° (Merlino et al. 2001). For Al-free tobermorite the $\nu_{Si-O}(max)$ value is in the range of 1200–

351   1215 cm^{-1}. In the IR spectra of minerals belonging to the palygorskite and the sepiolite groups and

352   structurally related minerals ("palysepioles", with $\varphi_{SiOSi} \approx 180°$ at the stacking of bands of

353   tetrahedra: Cámara et al. 2002; Ferraris and Gula 2005; Chukanov et al. 2012) $\nu_{Si-O}(max)$ varies

15

354   from 1160 to 1212 cm^{-1}. Another example is suolunite $Ca_2[Si_2O_5(OH)_2] \cdot H_2O$ (Ma et al. 1999) with

355   φ_{SiOSi} = 180°, ν_{Si-O}(max) = 1191 cm^{-1}. In contrast to these examples, for cuspidine $Ca_8(Si_2O_7)_2F_4$

356   (Saburi et al. 1977) φ_{SiOSi} = 155.4°, ν_{Si-O}(max) = 1057 cm^{-1}; for kilchoanite $Ca_6(Si_3O_{10})(SiO_4)$

357   (Taylor 1971) φ_{SiOSi} = 117°, ν_{Si-O}(max) = 1047 cm^{-1}.

358   The presence of the bands at 1120 and 1167 cm^{-1} in the IR spectrum of paratobermorite

359   (unlike tobermorite: Fig. 7b) indicates the presence of two kinds of the Si–O–Si bridges with large

360   (but significantly smaller than 180°) Si–O–Si angles and is in good agreement with the values of the

361     $T4–OT4–T4$ and $T3–OT3–T3$ angles [161(2)° and 174.0(12)°, respectively]. Unlike, the IR spectra

362   of tobermorite contain a single band in the range of 1160–1220 cm^{-1} (typically, 1200 ± 20 cm^{-1}:

363   Chukanov 2014) which corresponds to a Si–O–Si angle close to 180°.

364   As compared to tobermorite, paratobermorite is characterized by lower wavenumbers of the

365   bands corresponding to O–H stretching vibrations and, consequently, by stronger hydrogen bonds.

366   Based on the correlation reported by Libowitzky (1999), the D$\cdots$A distances for hydrogen bonds in

367   paratobermorite corresponding to the bands at 3220, 2446, and 3538 cm^{-1} are equal to 2.71, 2.83, and

368   2.97 Å, respectively. Bands of carbonate and orthoborate anions are not observed in the IR spectrum

369   of paratobermorite.

370

371   **X-ray diffraction data and crystal structure**

372   Powder XRD data of paratobermorite are given in Table 3. Parameters of the monoclinic unit

373   cell calculated from powder data are: a = 11.245 (3), b = 7.391 (2), c = 23.01 (1) Å, γ = 90.00 (5)°

374   and V = 1912 (2) Å^3.

375   The unit-cell parameters obtained for paratobermorite from single-crystal XRD data are: a =

376   11.2220 (4), b = 7.3777 (2), c = 22.9425 (8) Å, γ = 89.990 (3)°, and V = 1899.46 (10) Å^3.

377   The crystal structure description of paratobermorite is reported here for the model in the

378   space group $C112_1/m$. Selected interatomic distances are given in Table 4 and bond valence

379   calculations in Table 5.

380   The crystal structure of paratobermorite (Fig. 2), like structures of other 'tobermorites 11 Å'

381   (Merlino et al. 2001), is based on the complex module built of sheet of Ca-centred polyhedra,

382   parallel to (001), with chains of T tetrahedra running along the b axis and attached to Ca-sheet.

383   Paratobermorite possesses the *complex module of type A* (Fig. 1a). There are three main T sites;

384   according to interatomic distances, $T1$ and $T2$ are fully occupied by Si atoms while the $T3$ site, as

385   well as the additional $T4$ site (these sites could be only alternatively occupied due to a short $T3$–$T4$

386   distance) are filled by Al and Si in the ratio 1:1; the site occupancy factors of $T3$ and $T4$ are 0.70 and

387   0.30, respectively. The chains of tetrahedra belonging to neighboring complex modules share

388   common oxygen vertices of the bridging $T3,4$ tetrahedra to form double chains (xonotlite-type

389   ribbons); in general, the heteropolyhedral Ca-T-O scaffolding appears as a microporous quasi-

390   framework. Two main Ca sites (Ca1 and Ca2) occupy seven-fold polyhedra which build the (001)

391   layers of the complex module. Wide channels in the quasi-framework contain two sites partially

392   occupied with Ca (additional Ca sites labelled as Ca3 and Ca4 in Tables 4 and 5 and Fig. 2) and five

393   partially occupied H_2O sites. Water molecules (labelled as Ow1–Ow5 in Tables 4 and 5) are placed

394   on the m plane and for better clarity their further site splitting and positional disorder were forbidden

395   during the refinement. In terms of polytypism (Merlino and Bonaccorsi 2008; Biagioni et al. 2015),

396   paratobermorite is represented by the $2M$ polytype.

397

Comparison of paratobermorite with other tobermorite-supergroup minerals

399   Paratobermorite belongs to 'tobermorites 11 Å', as well as tobermorite, kenotobermorite and

400   clinotobermorite. All known polytypes of these minerals are reported in Table 1.

17

401   Based on the structure arrangement, paratobermorite is included in the tobermorite group

402   within the tobermorite supergroup, together with tobermorite and kenotobermorite. The belonging of

403   paratobermorite to the tobermorite group is justified by the same type of tetrahedral motif in the

404   structure (Fig. 8a,b) whereas clinotobermorite (Fig. 8c) and other tobermorite-supergroup members

405   differ from them in this aspect and, thus, do not belong to the tobermorite group (Biagioni et al.

406   2015).

407   The peculiar aspects which characterize paratobermorite as an individual mineral species and

408   distinguish it from tobermorite and other related minerals, are as follows.

409   (1) The essential building units of the crystal structures of paratobermorite and related

410   minerals are topologically different. The complex Ca-T-O layer in the structure of paratobermorite is

411   the *complex module of type A* (Fig. 1a) whereas the complex Ca-T-O layer in tobermorite is the

412   *complex module of type B* (Fig. 1b). They significantly differ from each other in the mutual

413   arrangement of T tetrahedra and Ca polyhedra (see above). From clinotobermorite, paratobermorite

414   significantly differs in the general topological characteristics of the tetrahedral motif (Figs. 8a,c).

415   Tobermorite differs from both these minerals in this aspect (Fig. 8b).

416   (2) In terms of crystal chemistry, paratobermorite differs from all other tobermorite-

417   supergroup minerals in the Al-Si ordering: it is not the only mineral significantly enriched with Al

418   but it is the first member of the group in which Al-Si ordering is found. The bridging T3,4 tetrahedra

419   which connect adjacent complex layers in the whole structure are occupied by Si and Al atoms in

420   the ratio 1:1 whereas the T1,2 tetrahedra are occupied by Si (Tables 4 and 5, Figs. 1, 2 and 8). All

421   other structurally studied minerals of the tobermorite-supergroup display Si-Al disorder: in their

422   structures, all T tetrahedra are essentially Si-dominant (Merlino et al. 1999, 2000, 2001; Bonaccorsi

423   et al. 2005 and references therein). For this reason, the simplified formula of paratobermorite

424    $Ca_5AlSi_5O_{16}(OH)\cdot5H_2O = Ca_5(AlSi)Si_4O_{16}(OH)\cdot5H_2O$, differs from all other valid minerals of the

425   tobermorite supergroup that have the simplified formulae with only Si in the tetrahedral part

18

426   (Biagioni et al. 2015; Table 1) and explains the larger value of the *c* parameter in comparison with

427   that of the other members of the tobermorite group.

428   (3) Paratobermorite differs from all other tobermorite-supergroup minerals in space group

429   and metrics of the unit cell that is a consequence of the above-discussed differences in the topology

430   of structure. The crystal data for 'tobermorites 11 Å' are summarized in Table 1 and the *ac*

431   projections of the chains of tetrahedra in the unit cells of tobermorite-2*M*, paratobermorite-2*M* and

432   clinotobermorite-2*M* (*i.e.*, monoclinic polytypes with $c = 22.5 – 23$ Å) are shown in Fig. 8.

433

434   **IMPLICATIONS**

435   Due to the original topological type of the crystal structure, paratobermorite can be

436   considered as a novel microporous material known only as a natural compound. Despite the fact that

437   it has not yet been synthesized, the discovery of paratobermorite at the Bazhenovskoe deposit makes

438   possible to study its properties. This finding has both scientific and applied value. On one hand, it

439   confirmed the previously predicted (Merlino and Bonaccorsi 2008) existence of a tobermorite-like

440   structure of this topological type. On the other hand, one can expect the presence of paratobermorite

441   as one of the phases in some cement materials (mainly in Portland cement), especially, materials

442   with a relatively high aluminum content. The upper limit of the substitution of Si for Al in

443   'tobermorites 11 Å' corresponds to the atomic ratio Al:(Al+Si) of 0.167 which corresponds to the

444   situation Si–O–Al around all O atoms bridging the wollastonite-type chains. In the case of

445   paratobermorite, this ratio is equal to 0.153, which exceeds the maximum Al:(Al+Si) values of 0.13

446   – 0.14 known for synthetic 'tobermorites' (Sakiyama et al. 2000). The formation of Al-rich

447   tobermorite-related compounds occurs most probably in some kinds of Al-rich cements containing

448   active SiO_2. Concretes and ceramics prepared from such cements show significant growth of

449   strength with time (El-Didamony et al. 2000; Chervonnyi et al. 2010). The ion-exchange capability

450   is mainly exhibited by Al-substituted tobermorite-related compounds (Bonaccorsi and Merlino

19

451   2005). In particular, these compounds show sorption capacity for a number of transition metals (Al-

452   Wakeel et al. 2001) and a high selectivity for Cs^+ and Li^+ (Tsuji et al. 1991 and references therein).

453   Thus, paratobermorite can be considered as a perspective prototype of microporous materials with

454   technologically important properties (cation-exchanger), probably better than ordinary, Al-poor

455   tobermorites.

456

457   ACKNOWLEDGMENTS

464

465   REFERENCES CITED

466

467   Al-Wakeel, E.I., El-Korashi, S.A., El-Hamaly, S.A., and Rizk, M.A. (2001) Divalent ion uptake of

468   heavy metal cations by (aluminium + alkali metals)-substituted synthetic 1.1 nm tobermorites.

469   Journal of Materials Science, 36, 2405–2415.

470   Biagioni, C., Merlino, S., and Bonaccorsi, E. (2015) The tobermorite supergroup: a new

471   nomenclature. Mineralogical Magazine, 79, 485–495.

472   Bonaccorsi, E. and Merlino, S. (2005) Modular microporous minerals: cancrinite-davyne group and

473   C-S-H phases. Reviews in Mineralogy and Geochemistry. Micro- and Mesoporous Mineral

474   Phases. Eds: G. Ferraris and S. Merlino, 57, 241–290.

475 Britvin, S.N., Dolivo-Dobrovolsky, D.V., and Krzhizhanovskaya, M.G. (2017) Software for

476   processing the X-ray powder diffraction data obtained from the curved image plate detector of

477   Rigaku RAXIS Rapid II diffractometer. Zapiski Rossiiskogo Mineralogicheskogo

478   Obshchestva, 146(3), 104–107 (in Russian).

479 Cámara, F., Garvie, L.A.J., Devouard, B., Groy, T.L., and Buseck, P.R. (2002) The structure of Mn-

480   rich tuperssuatsiaite: a palygorskite-related mineral. American Mineralogist, 87, 1458–1463.

481 Chervonnyi, A.D., Chukanov, N.V., and Chervonnaya, N.A. (2010) Synthetic calcium

482   aluminosilicate monolith: III. The nature of binder and high-temperature behavior. Russian

483   Journal of Inorganic Chemistry, 55. 1521–1528.

484 Chukanov, N.V. (2014) Infrared Spectra of Mineral Species: Extended Library. Springer-Verlag,

485   Dordrecht, 1716 pp.

486 Chukanov, N.V. and Chervonnyi, A.D. (2016) Infrared Spectroscopy of Minerals and Related

487   Compounds. Springer Verlag, Cham, 1109 pp.

488 Chukanov, N.V., Britvin, S.N., Blass, G., Belakovskiy, D.I., and Van, K.V. (2012) Windhoekite,

489      $Ca_2Fe^{3+}_{3-x}(Si_8O_{20})(OH)_4 \cdot 10H_2O$, a new palygorskite-group mineral from the Aris phonolite,

490   Namibia. European Journal of Mineralogy, 24, 171–179.

491 Churakov, S.V. (2009) Structural position of H_2O molecules and hydrogen bonding in anomalous

492   11Å tobermorite. American Mineralogist, 94, 156–165.

493 Claringbull, G.F. and Hey, M.H. (1952) A reexamination of tobermorite. Mineralogical Magazine,

494   29, 960–962.

495 Dornberger-Schiff, K. (1956) On the order-disorder (OD-structures). Acta Crystallographica, 9, 593.

496 Dornberger-Schiff, K. (1964) Grundzüge einer Theorie von OD-Strukturen aus Schichten.

497   Abhandlungen der Deutschen Akademie der Wissenschaften zu Berlin. Klasse für Chemie,

498   Geologie und Biologie, 3, 1–107.

499 Dornberger-Schiff, K. (1966) Lehrgang über OD-Strukturen, Akademie-Verlag, Berlin, 135 pp.

21

500   Dornberger-Schiff, K. and Fichtner, K. (1972) On the symmetry of OD-structures consisting of

501   equivalent layers. Kristall und Technik, 7, 1035–1056.

502   El-Didamony, H., Khalil, K.A., and El-Attat, M.S. (2000) Physicochemical characteristics of fired

503   clay-limestone mixtures. Cement and Concrete Research, 30, 7–11.

504   Erokhin, Yu.V. (2017) Bazhenovskoe Deposit (Central Urals, Russia): Mineralogy of Rodingites.

505   Mineralogical Almanac, 22(3), 1–136.

506   Ferraris, G. and Gula, A. (2005) Polysomatic aspects in microporous minerals –

507   heterophyllosilicates, palysepioles and rhodesite-related structures. Reviews in Mineralogy and

508   Geochemistry. Micro- and Mesoporous Mineral Phases, 57, 69–104.

509   Ferraris, G., Makovicky, E. and Merlino, S. (2008) Crystallography of Modular Materials. Oxford,

510   IUCr/Oxford University Press.

511   Gagné, O.C. and Hawthorne, F.C. (2015) Comprehensive derivation of bond-valence parameters for

512   ion pairs involving oxygen. Acta Crystallographica, B71, 562–578.

513   Hamid, S.A. (1981) The crystal structure of the 11Å natural tobermorite

514        $Ca_{2.25}[Si_3O_{7.5}(OH)_{1.5}]\cdot 1H_2O$. Zeitschrift für Kristallographie, 154, 189–198.

515   Heddle, M.F. (1880) Preliminary notice of substances which may prove to be new minerals.

516   Mineralogical Magazine, 4, 117–123.

517   Henmi, C. and Kusachi, I. (1992) Clinotobermorite, $Ca_5Si_6(O,OH)_{18}\cdot 5H_2O$, a new mineral from

518   Fuka, Okayama Prefecture, Japan. Mineralogical Magazine, 56, 353–358.

519   Hoffmann, C. and Armbruster, T. (1997) Clinotobermorite, $Ca_5[Si_3O_8(OH)]_2\cdot 4H_2O$ –

520        $Ca_5[Si_6O_{17}]\cdot 5H_2O$, a natural C-S-H(I) type cement mineral: determination of the substructure.

521   Zeitschrift für Kristallographie, 212, 864–873.

522   Kudoh, Y. and Takéuchi, Y. (1979) Polytypism in xonotlite: (I) Structure of an A-1 polytype,

523   locality: Heguri, Chiba Prefecture, Japan. Mineralogical Journal (Japan), 9, 349–373.

524 Libowitzky, E. (1999) Correlation of O–H stretching frequencies and O–H⋯O hydrogen bond

525   lengths in minerals. Monatshefte für Chemie, 130, 1047–1059.

526 Ma, Z., Shi, N., Mou, G., and Liao, L. (1999) Crystal structure refinement of suolunite and its

527   significance to the cement techniques. Chinese Science Bulletin, 44, 2125–2130.

528 Mamedov, Kh.S and Belov, N.V. (1958) On the crystal structure of tobermorite (tobermorites).

529   Doklady Akademii Nauk SSSR, 123(1), 163–165 (in Russian).

530 Mandarino, J.A. (1981) The Gladstone-Dale relationship, Part IV. The compatibility concept and its

531   application. The Canadian Mineralogist, 19, 441–450.

532 McConnell, J.D.C. (1954) The hydrated calcium silicates riversideite, tobermorite, and plombierite.

533   Mineralogical Magazine, 30, 293–305.

534 Megaw, H.D. and Kelsey, C.H. (1956) Crystal structure of tobermorite. Nature, 177, 390–391.

535 Merlino, S. and Bonaccorsi, E. (2008) Double wollastonite chains: topological/conformational

536   varieties, polytypic forms, isotypic compounds. Zeitschrift für Kristallographie, 223, 85–97.

537 Merlino, S., Bonaccorsi, E., and Armbruster, T. (1999) Tobermorites: Their real structure and order-

538   disorder (OD) character. American Mineralogist, 84, 1613–1621.

539 Merlino, S., Bonaccorsi, E., and Armbruster, T. (2000) The real structures of clinotobermorite and

540   tobermorite 9 Å: OD character, polytypes, and structural relationships. European Journal of

541   Mineralogy, 12, 411–429.

542 Merlino, S., Bonaccorsi, E., and Armbruster, T. (2001) The real structure of tobermorite 11Å:

543   normal and anomalous forms, OD character and polytypic modifications. European Journal of

544   Mineralogy, 13, 577–590.

545 Organova, N.I., Koporulina, E.V., Ivanova, A.G., Trubkin, N.V. Zadov, A.E., Khomyakov, A.P.,

546   Marcille, I.M., Chukanov, N.V., and Shmakov, A.N. (2002) Structure model of Al,K-

547   substituted tobermorite and structural changes upon heating. Crystallography Reports, 47(6),

548   950–956.

23

549   Pekov, I.V., Zubkova, N.V., Chukanov, N.V., Yapaskurt, V.O., Britvin, S.N., Kasatkin, A.V., and

550   Pushcharovsky D.Y. (2019) Oyelite: new mineralogical data, crystal structure model and

551   refined formula $Ca_5BSi_4O_{13}(OH)_3 \cdot 4H_2O$. European Journal of Mineralogy, 31, 595–608.

552   Richardson, L.G. (2008) The calcium silicate hydrates. Cement and Concrete Research, 38, 137–

553   158.

554   Rigaku Oxford Diffraction (2018) CrysAlisPro Software System, v. 1.171.39.46, Rigaku

555   Corporation, Oxford, UK.

556   Saburi, S., Kawahara, A., Henmi, C., Kusachi, I., and Kihara, K. (1977) The refinement of the

557   crystal structure of cuspidine. Mineralogical Journal, 8(5), 286–298.

558   Sakiyama, M., Maeshima, T., and Mitsuda, T. (2000) Synthesis and crystal chemistry of Al-

559   substituted 11 Å tobermorite. Journal of the Society of Inorganic Materials of Japan, 7, 413–

560   419.

561   Sheldrick, G.M. (2015) Crystal structure refinement with SHELXL. Acta Crystallographica, C71, 3–

562   8.

563   Spek, A.L. (2003) Single-crystal structure validation with the program PLATON. Journal of

564   Applied Crystallography, 36, 7–13.

565   Taylor, H.F.W. (1953) Hydrated calcium silicates. Part V. The water content of calcium silicate

566   hydrate (I). Journal of the Chemical Society, 12, 163–171.

567   Taylor, H.F.W. (1964) The calcium silicate hydrates. Chemistry of Cements. Vol. 1. (ed. H.F.W.

568   Taylor). Academic Press, London, 167–232.

569   Taylor, H.F.W. (1971) The crystal structure of kilchoanite. Mineralogical Magazine, 38, 26–31.

570   Tsuji, M., Komarneni, S., and Malla, P. (1991) Substituted tobermorites: ^{27}Al and ^{29}Si MASNMR,

571   cation exchange, and water sorption studies. Journal of American Ceramic Society, 74, 274–

572   279.

573   Zadov, A.E., Chukanov, N.V., Organova, N.I., Belakovskiy, D.I., Fedorov, A.V., Kartashov, P.M.,

574   Kuz'mina O.V., Litsarev, M.A., Mokhov, A.V., Loskutov, A.B., and Fin'ko, V.I. (1995) New

575   finds and studies of tobermorite-group minerals. Zapiski Vserossiiskogo Mineralogicheskogo

576   Obshchestva, 124(2), 36–54 (in Russian).

577   Zadov, A.E., Chukanov, N.V., Organova, N.I., Kuz'mina O.V., Belakovskiy, D.I., Nechay, V.G.,

578   Sokolovskiy, F.S., and Kuznetsova, O.Yu. (2000) Comparative study of rosenhahnite from

579   California and Urals. Refinement of formula. Zapiski Vserossiiskogo Mineralogicheskogo

580   Obshchestva, 129(2), 85–96 (in Russian).

581   Zadov, A.E., Chukanov, N.V., Organova, N.I., Kuz'mina O.V., Belakovskiy, D.I., Litsarev, M.A.,

582   Nechay, V.G., and Sokolovskiy, F.S. (2001) Hydration, dehydration and thermal

583   transformations of tobermorite-group minerals. Zapiski Vserossiiskogo Mineralogicheskogo

584   Obshchestva, 130(2), 26–40 (in Russian).

585   Zadov, A.E., Grabezhev, A.I., Pertsev, N.N., Chukanov, N.V., and Pribavkin, S.V. (2006)

586   Tobermorite-plombierite metasomatites of the Gumeshevsk skarn-porphyry copper deposit, middle

587   Urals. Doklady Earth Sciences, 407(2), 495–497.

588   **Figure captions**

589

590   **Figure 1.** Two topological types of the complex Ca-*T*-O module, a fundamental building unit in the

591   crystal structures of tobermorite-supergroup minerals: (a) complex module of type A in

592   paratobermorite and (b) complex module of type B in tobermorite (drawn after Merlino et al. 2001).

593

594   **Figure 2.** The crystal structure of paratobermorite (a) and tobermorite (drawn after Merlino et al.

595   2001) (b). The unit cells are outlined.

596

597   **Figure 3.** OD Layer in tobermorite 11Å (taken from Merlino et al., 2001). The λ operations are

598   indicated.

599

600   **Figure 4.** Paratobermorite crystal.

601

602   **Figure 5.** Crystals (a, b) and open-work crystal cluster of paratobermorite. SEM images: a – BSE

603   mode, b and c – SE mode.

604

605   **Figure 6.** Paratobermorite aggregates: a – open-work aggregates on almost colourless grossular

606   crystal crust with small milky-white spherulites of pectolite-1*A* (photo: I.V. Pekov & A.V.

607   Kasatkin); b – radial cluster of prismatic crystals (length of the largest, divergent crystal is 8 mm) on

608   prehnite spherulitic crust, which covers a wall of cavity in grossular rodingite (photo: N.N.

609   Koshlyakova). FOV width: a – 7.5 mm, b – 1.5 cm.

610

611　**Figure 7.** Powder infrared absorption spectra of (*a*) paratobermorite and (*b*) Al-free tobermorite-2*M*

612　with the empirical formula $Ca_{4.68}Si_6O_{16.36}(OH)_{0.64} \cdot nH_2O$ (*n* ~ 5) from the Pervomaiskiy quarry, Mt.

613　Bol'shoy Kermen, Bakhchisaray district, Crimea Peninsula.

614

615　**Figure 8.** Tetrahedral motifs in the structures of 2*M* polytypes of 'tobermorites 11 Å':

616　paratobermorite (a; for legend see Fig. 2; *T*3- and *T*4-centred tetrahedra are filled alternatively and

617　*T*4 tetrahedra are not shown here for better clarity), tobermorite (b; drawn after Merlino et al. 2001)

618　and clinotobermorite (c; drawn after Merlino et al. 2000). The unit cells are outlined.

619
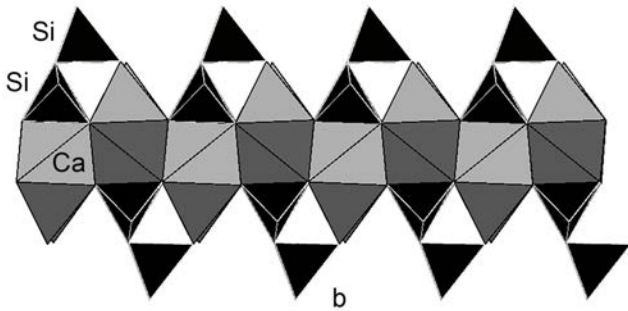
(Al,Si)

Si

Ca

a

620
621
622

Figure 1a

Si

Si

Ca

b

623
624
625

Figure 1b

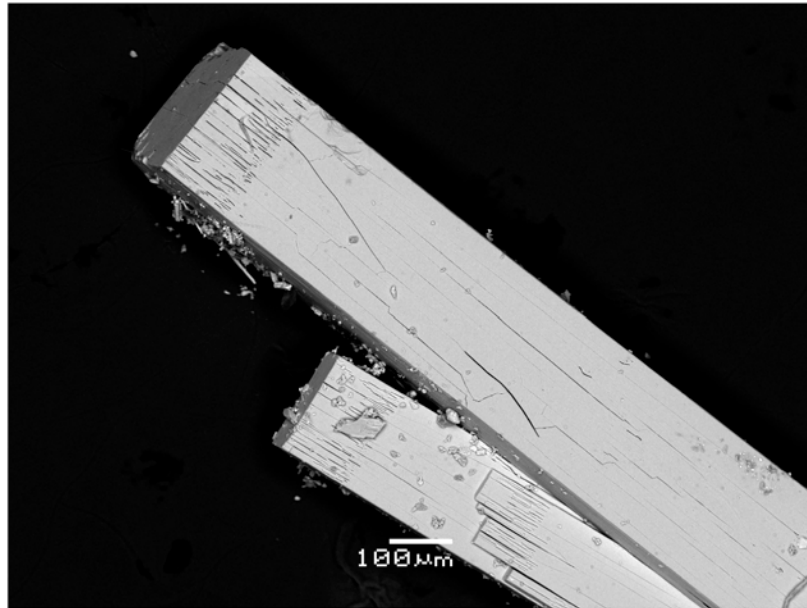626

Figure 2a

627

Figure 2b
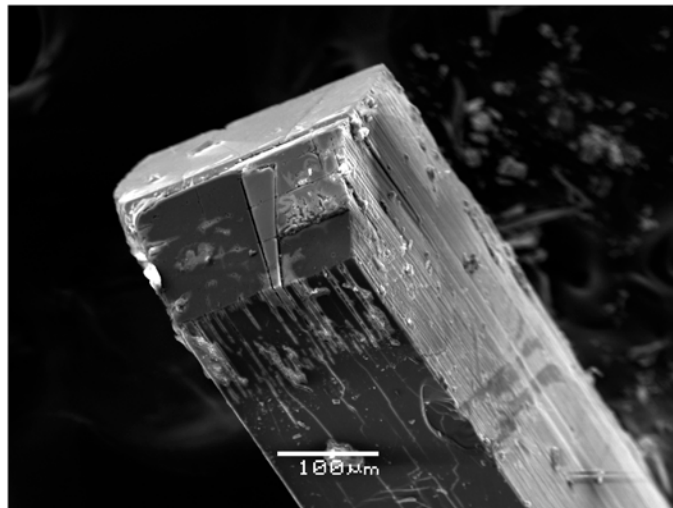
628

Figure 3

629

Figure 4
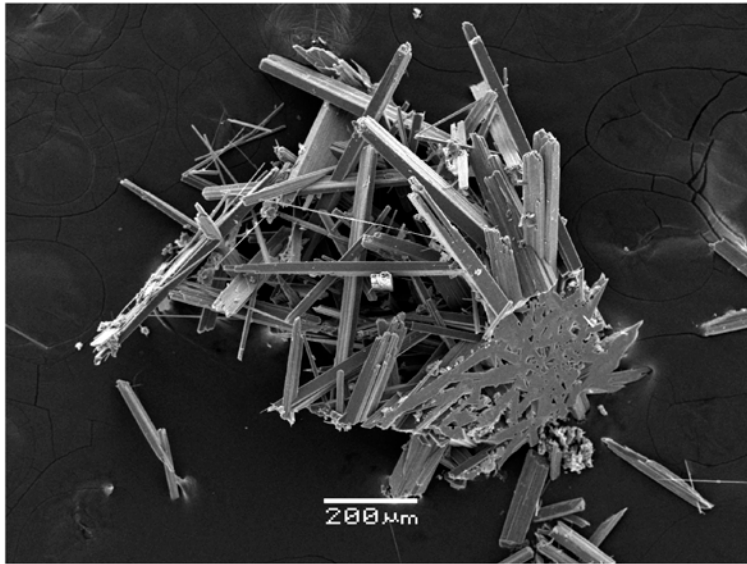
630
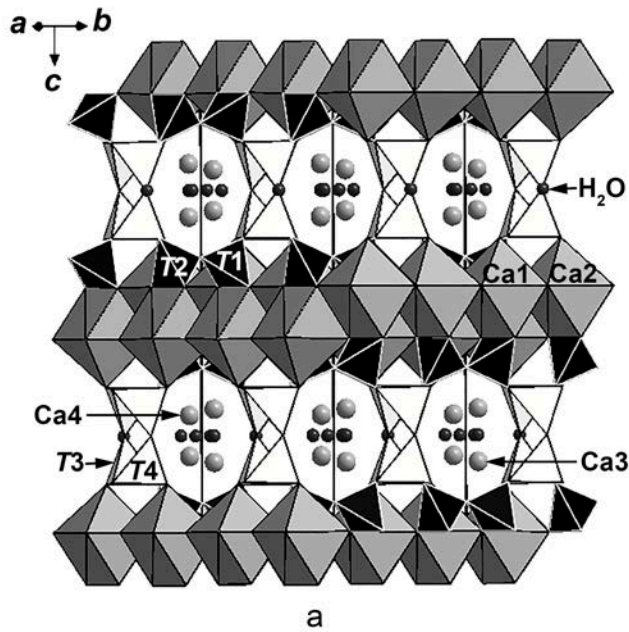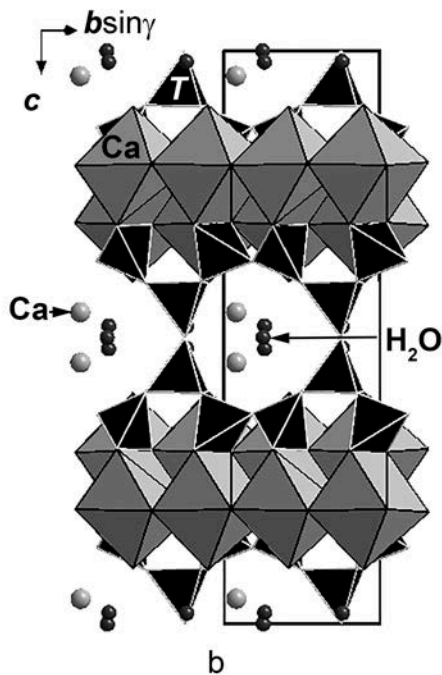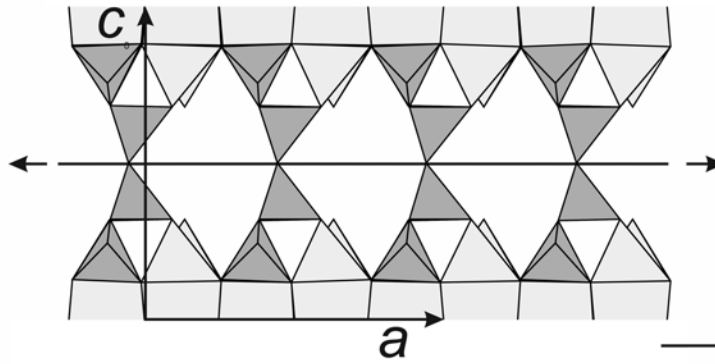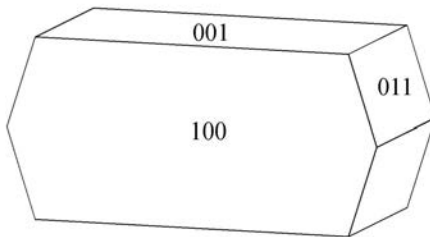
631

a

632   Figure 5a

b

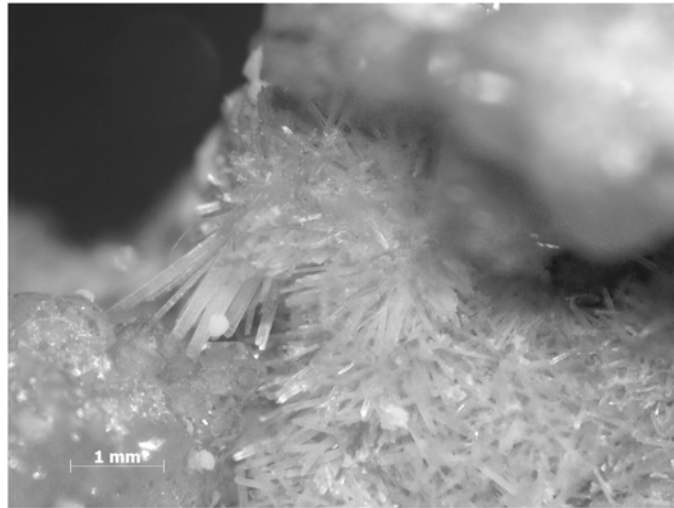633   Figure 5b
634
635
636

c

Figure 5c
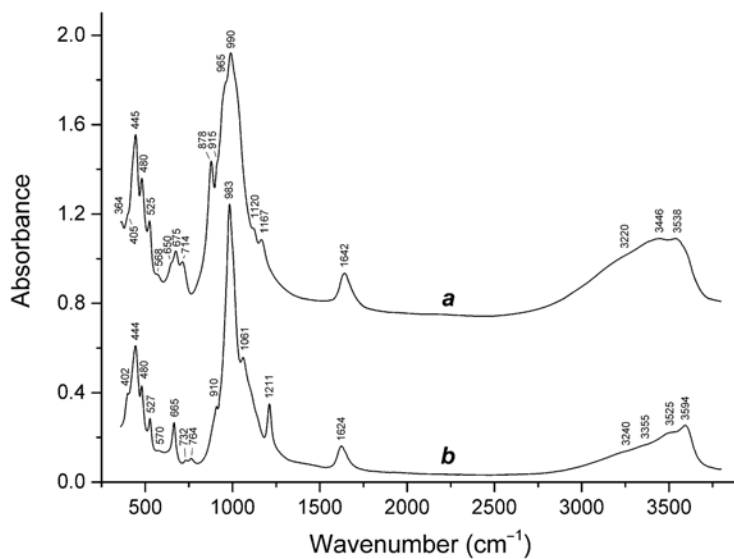
637
638
639

640

641

a

Figure 6a

642

b

Figure 6b

643
644
645

646

34

Figure 7

647

648

649
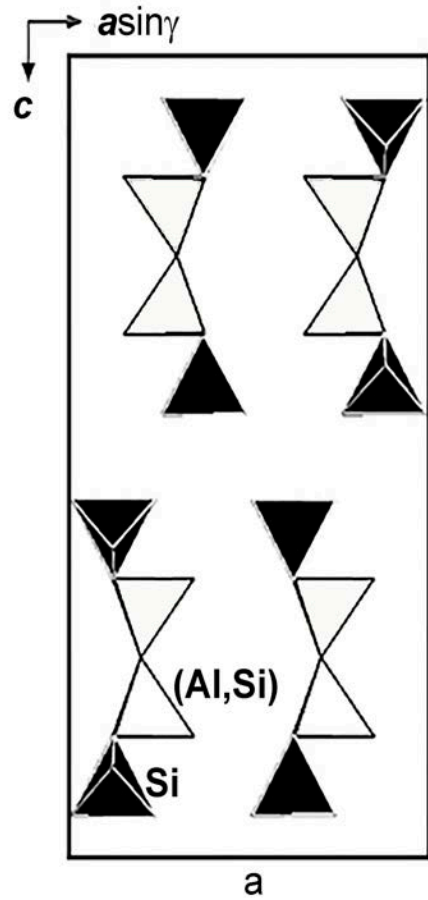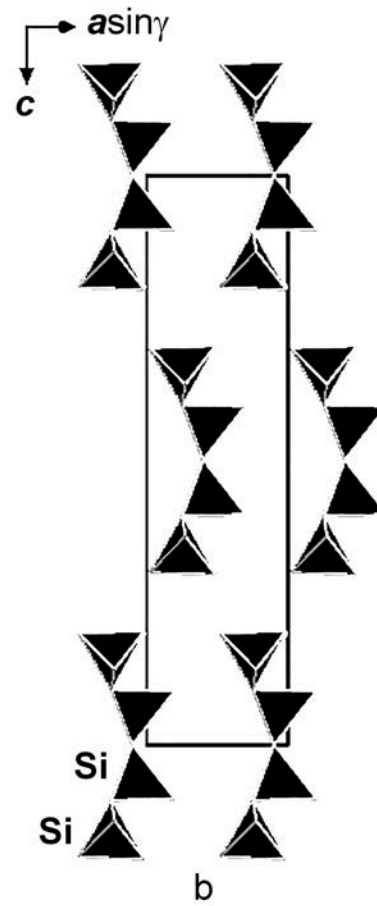
Figure 8a

Figure 8b
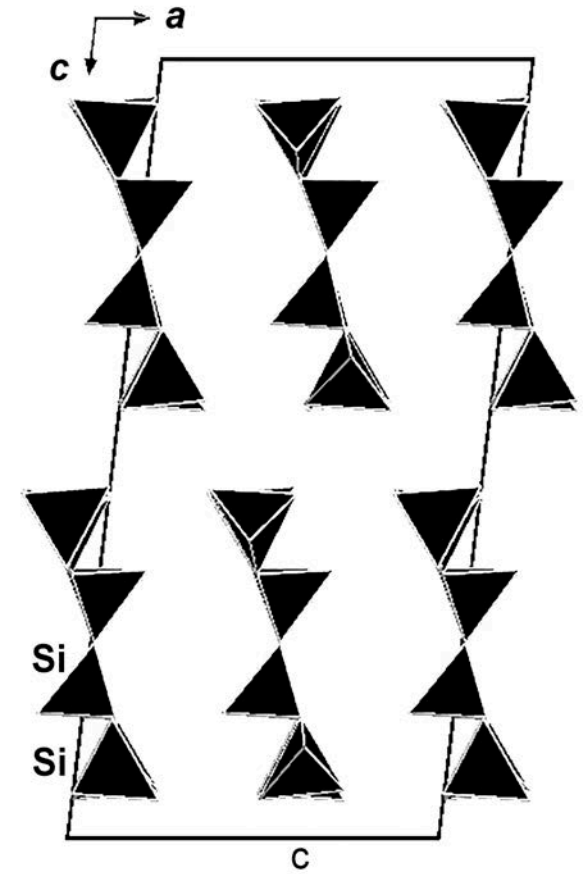
Figure 8c

651 **Tables**

652

653 **Table 1**. Crystal data of tobermorite-supergroup minerals belonging to 'tobermorites 11 Å': tobermorite, clinotobermorite, kenotobermorite
654 and paratobermorite (all polytypes known in nature are included)

655

Mineral	Paratobermorite	Tobermorite	Kenotobermorite		Clinotobermorite	
Simplified formula	$Ca_5AlSi_5O_{16}(OH)\cdot5H_2O$	$Ca_5Si_6O_{17}\cdot5H_2O$	$Ca_4Si_6O_{15}(OH)_2\cdot5H_2O$		$Ca_5Si_6O_{17}\cdot5H_2O$	
Ideal (structural) formula*	$[Ca_4(Al_{0.5}Si_{0.5})_2Si_4O_{16}(OH)\cdot2H_2O]$ $\cdot(Ca\cdot3H_2O)$	$[Ca_4Si_6O_{17}\cdot2H_2O]$ $\cdot(Ca\cdot3H_2O)$	$[Ca_4Si_6O_{15}(OH)_2\cdot2H_2O]\cdot(3H_2O)$		$[Ca_4Si_6O_{17}\cdot2H_2O]\cdot(Ca\cdot3H_2O)$	
Polytype	2*M*	2*M*	2*M*	4*O*	2*M*	1*A*
Crystal system Space group	Monoclinic *C*112$_1$/*m*	Monoclinic *B*11*m*	Monoclinic *B*11*m*	Orthorhombic *F*2*dd*	Monoclinic *Cc*	Triclinic *C*1
a, Å	11.2220 (4)	6.732	6.735	11.265	11.276	11.274
b, Å	7.3777 (2)	7.369	7.385	7.385	7.343	7.344
c, Å	22.9425 (8)	22.680	22.487	44.970	22.642	11.468
α, °	90	90	90	90	90	99.18
β, °	90	90	90	90	97.28	97.19
γ, °	89.990 (3)	123.18	123.25	90	90	90.02
V, Å^3	1899.46 (10)	942	935	3742	1860	930
Z	4	2	2	8	4	2
Source	This work	Merlino et al. 2001; Biagioni et al. 2015	Merlino et al. 1999, 2001; Biagioni et al. 2015		Merlino et al. 1999, 2000; Biagioni et al. 2015	

656 Unit cells of all listed minerals are given in the same setting corresponding to the orientation of layers of Ca-polyhedra in the *ab* plane.
657 Plombiérite ('tobermorite 14 Å') and insufficiently studied riversideite ('tobermorite 9 Å') are not included.
658 * Written in accordance with the IMA-accepted nomenclature of tobermorite-supergroup minerals (Biagioni et al. 2015).

659   **Table 2**. Chemical composition (wt.%) of paratobermorite

Constituent	Mean*	Range	Stand. Dev. (σ)	Probe standard
Na_2O	0.40	0.29 – 0.47	0.08	NaCl
K_2O	0.28	0.23 – 0.33	0.04	microcline
CaO	36.60	36.26 – 36.82	0.26	plagioclase
MnO	0.04	0.00 – 0.11	0.04	$MnTiO_3$
BaO	0.07	0.00 – 0.14	0.06	BaF_2
Al_2O_3	6.46	6.30 – 6.72	0.19	plagioclase
SiO_2	42.32	42.03 – 42.71	0.32	diopside
H_2O	14.10	13.83 – 14.37		
Total	100.27			

660   * Averaged for four spot analyses. Contents of other elements with atomic numbers higher than that
661   of carbon are below detection limits.

662

663

664   **Table 3**. Powder X-ray diffraction data (*d* in Å) of paratobermorite

I_{obs}	d_{obs}	I_{calc}*	d_{calc}**	h k l
100	**11.52**	100	11.471	002
5	6.17	1	6.165	110
5	5.97	1, 1	5.954, 5.954	111, -111
3	5.76	3	5.736	004
24	**5.46**	17, 1, 2	5.450, 5.431, 5.431	201, 112, -112
2	4.808	3	4.800	113
3	3.836	2	3.824	006
4	3.650	2, 3	3.681, 3.642	115, 021
17	**3.562**	13	3.552	205
11	3.329	1, 5, 1	3.337, 3.323, 3.302	310, 023, 311
4	3.259	6	3.249	-116
3	3.211	1	3.204	312
51	**3.088**	18, 16, 2	3.083, 3.083, 3.058	220, -220, -313
50	**2.982**	20, 14	2.977, 2.977	222, -222
10	2.878	3, 1, 1, 6	2.894, 2.884, 2.875, 2.868	117, 314, 025, 008
20	**2.838**	18	2.830	207
11	2.813	9	2.806	400
6	2.729	3, 1, 1	2.725, 2.715, 2.715	402, 224, -224
9	2.526	6	2.520	404
7	2.456	6	2.450	027
9	2.328	9	2.321	209
7	2.302	7	2.294	0.0.10
10	2.148	3, 4	2.144, 2.144	423, -423
7	2.104	2, 1, 3	2.100, 2.100, 2.097	228, -228, 029
14	**2.013**	7, 6	2.008, 2.008	425, -425
22	**1.848**	5, 9, 11, 2, 2	1.846, 1.846, 1.844, 1.840, 1.840	427, -427, 040, 2.2.10, -2.2.10
3	1.823	2	1.821	042
2	1.736	2	1.732	605
8	1.685	2, 4, 4	1.683, 1.680, 1.680	2.0.13, 429, -429
8	1.672	4, 4	1.668, 1.668	620, -620
3	1.641	1, 1	1.639, 1.637	0.0.14, -245
7	1.629	6	1.624	607
1	1.603	1	1.600	339
2	1.555	2	1.551	048
3	1.549	2, 2	1.545, 1.545	247, -247
1	1.530	1, 1	1.531, 1.528	-3.3.10, 442
1	1.480	1	1.476	2.0.15
3	1.447	1, 2	1.444, 1.444	249, -249
2	1.406	3	1.403	800
2	1.395	2	1.392	802

665   * For the calculated pattern, only reflections with intensities ≥1 are given; ** for the unit-cell
666   parameters calculated from single-crystal data; the strongest reflections are marked in bold.

667
668

669
670
671
672
673
674 **Table 4**. Selected interatomic distances (Å) in the structure of paratobermorite
675

Ca1 – O1	2.315(7)	Ca3 – Ow3	2.05(5)
– O2	2.360(7)	– O7	2.126(12)
– O3	2.405(8)	– Ow2	2.30(5)
– O4	2.423(8)	– Ow4	2.32(7)
– O1	2.505(6)	– O8	2.328(11)
– O9	2.545(11)	– O6	2.720(14)
– O2	2.547(6)	– O5	2.775(14)
Ca2 – O4	2.340(8)	Ca4 – Ow5	2.04(6)
– O3	2.360(8)	– O9	2.24(2)
– O2	2.451(7)	– Ow1	2.25(3)
– O8	2.461(8)	– O7	2.49(2)
– O1	2.477(7)	– O6	2.85(2)
– O4	2.550(6)	– O5	2.98(2)
– O3	2.612(7)		
$T1$ – O3	1.603(6)	$T3$ – O$T3$	1.634(3)
– O4	1.612(6)	– O6	1.698(9)
– O5	1.615(8)	– O5	1.721(9)
– O7	1.639(8)	– O8	1.728(9)
$T2$ – O2	1.565(6)	$T4$ – O6	1.694(12)
– O1	1.603(6)	– O$T4$	1.705(9)
– O6	1.645(7)	– O5	1.704(12)
– O7	1.649(8)	– O9	1.806(12)

676
677

678 **Table 5**. Bond-valence calculations for paratobermorite
679

Site	Ca1	Ca2	$T1$	$T2$	$T3 =$ $Al_{0.35}Si_{0.35}$	$T4 =$ $Al_{0.15}Si_{0.15}$	Ca3 = $Ca_{0.25}$	Ca4 = $Ca_{0.125}$	Σ
O1 = O	0.37 0.23	0.25		1.06					1.91
O2 = O	0.33 0.21	0.26		1.16					1.96
O3 = O	0.30	0.33 0.18	1.06						1.87
O4 = O	0.28	0.35 0.21	1.03						1.87
O5 = O			1.02		0.55	0.25	0.03	0.01	1.86
O6 = O				0.95	0.60	0.26	0.03	0.01	1.85
O7 = O			0.96	0.94			0.14	0.03	2.07
O8 = $O_{0.25}(OH)_{0.45}(H_2O)_{0.3}$		0.26			0.55		0.09		0.90
O9 = $(OH)_{0.3}(H_2O)_{0.7}$	0.21					0.19		0.06	0.46
$OT3 = O_{0.70}$					$0.69^{x2\rightarrow}$				1.38
$OT4 = O_{0.30}$						$0.25^{x2\rightarrow}$			0.50
Ow1 = $H_2O_{0.50}$								0.05 x2→	0.10
Ow2 = $H_2O_{0.50}$							0.10 x2→		0.20
Ow3 = $H_2O_{0.50}$							0.18 x2→		0.36
Ow4 = $H_2O_{0.50}$							0.09 x2→		0.18
Ow5 = $H_2O_{0.50}$								0.09 x2→	0.18
Σ	1.93	1.84	4.07	4.11	2.39	0.95	0.66	0.25	

680 Bond-valence parameters were taken from Gagné and Hawthorne (2015).